Agricultural and Forest Meteorology 285–286 (2020) 107911

Contents lists available at ScienceDirect

Agricultural and Forest Meteorology

journal homepage: www.elsevier.com/locate/agrformet

A dynamic model of RuBP-regeneration limited photosynthesis accounting for photoinhibition, heat and water stress

Nicolas Bambach[a,*], Kyaw Tha Paw U[a], Matthew E Gilbert[b]

[a] Department of Land, Air and Water Resources, University of California Davis, Mail Stop One, Davis, CA, United States
[b] Department of Plant Sciences, University of California Davis, Mail Stop One, Davis, CA, United States

ARTICLE INFO

Keywords:
Chlorophyll fluorescence
Non-photochemical quenching
Maximum quantum efficiency

ABSTRACT

Plant physiological responses to stress and subsequent damage have not been successfully integrated into leaf, plant or land surface models. Water deficit leads to a series of plant responses: stomatal closure decreases evaporative cooling leading to higher leaf temperature, which it can affect photosynthetic dissipation of absorbed energy, especially under high irradiance. Excess absorbed energy by PSII results in photoinhibition, which is not typically included when modeling photosynthesis using the Farquhar-von Caemmerer-Berry (FvCB) model. We introduce a novel approach to represent plant-atmosphere interactions: a non-steady state model of photoinhibition linked to the RuBP-regeneration component of the FvCB model that accounts for the interactions between high temperature, irradiance, and water deficits. Gas exchange and chlorophyll fluorescence dynamics showed that, under severe water stress, the maximum quantum efficiency of PSII (F_v/F_m) quickly decreases, and it takes days to recover. We found a clear relationship between maximum electron transport rate and F_v/F_m and that short-term acclimation to irradiance affected photosynthetic FvCB model parameters. F_v/F_m functioned well as a coupling variable, able to scale RuBP-regeneration limited photosynthesis parameters proportional to photoinhibition. These results indicate that plant stress, photo-inhibitory damage, and recovery can be explicitly represented when modeling photosynthesis.

1. Introduction

Photosynthesis is the result of both biophysical processes, such as radiation absorption and energy transfer to reaction centers; and biochemical processes, such as the binding of CO_2 by Rubisco (Barber, 2009; Farquhar et al., 1980). These processes are closely regulated by environmental stress factors such as low CO_2 concentration, water deficits, high irradiance and high/low temperature (Berry and Downton, 1982). Farquhar et al. (1980) proposed a mechanistically based C3 photosynthesis model (FvCB), which allows the prediction of carbon uptake under a wide range of environmental conditions. Under water deficit, leaf temperatures may exceed the optimal range leading to large photosynthesis decreases above 40 °C (Lin et al., 2012). Some of the observed decline in photosynthesis is due to RuBP-regeneration limitations (June et al., 2004; Zhou et al., 2014), representing either negative temperature responses of the thylakoid membrane components, or photoinhibitory dissipation of energy (von Caemmerer, 2000). While the FvCB model is sensitive to these stress factors, the effects are modeled in steady state (without "memory"), leading to no lasting effects upon cessation of the stress.

Absorbed irradiance (W_{abs}) excites chlorophyll molecules in PSII and de-excitation of this energy is attained through three complementary processes: photochemistry (W_{photo}) mostly comprising of RuBP-regeneration, chlorophyll fluorescence (W_{fl}), and non-photochemical quenching (NPQ; W_{NPQ}). Conveniently, the activity of Photosystem II (PSII) can be assessed through chlorophyll fluorescence, measured by the Pulse Amplitude Modulation (PAM) approach (Demmig-Adams and Adams, 1996; Genty et al., 1989; Krause and Weis, 1991; Müller et al., 2001). Current PAM systems are capable of continuously measuring leaf-level fluorescence parameters on a number of plants for extended time periods. Besides, leaf-level gas exchange systems have been widely used in the last decades, resulting in several studies applying the FvCB approach to study steady-state photosynthesis. Nevertheless, fluorescence parameters, such as the quantum efficiency of PSII photochemistry, have not been directly linked to the FvCB approach to represent physiological responses to stress, and potentially, photoinhibition.

The objectives of this study were: (1) to develop a dynamic model of photoinhibitory effects on RuBP-regeneration photosynthetic limitations that accounts for the interactions between irradiance and

* Corresponding author.
E-mail address: nbambach@ucdavis.edu (N. Bambach).

https://doi.org/10.1016/j.agrformet.2020.107911
Received 7 December 2018; Received in revised form 21 January 2020; Accepted 22 January 2020

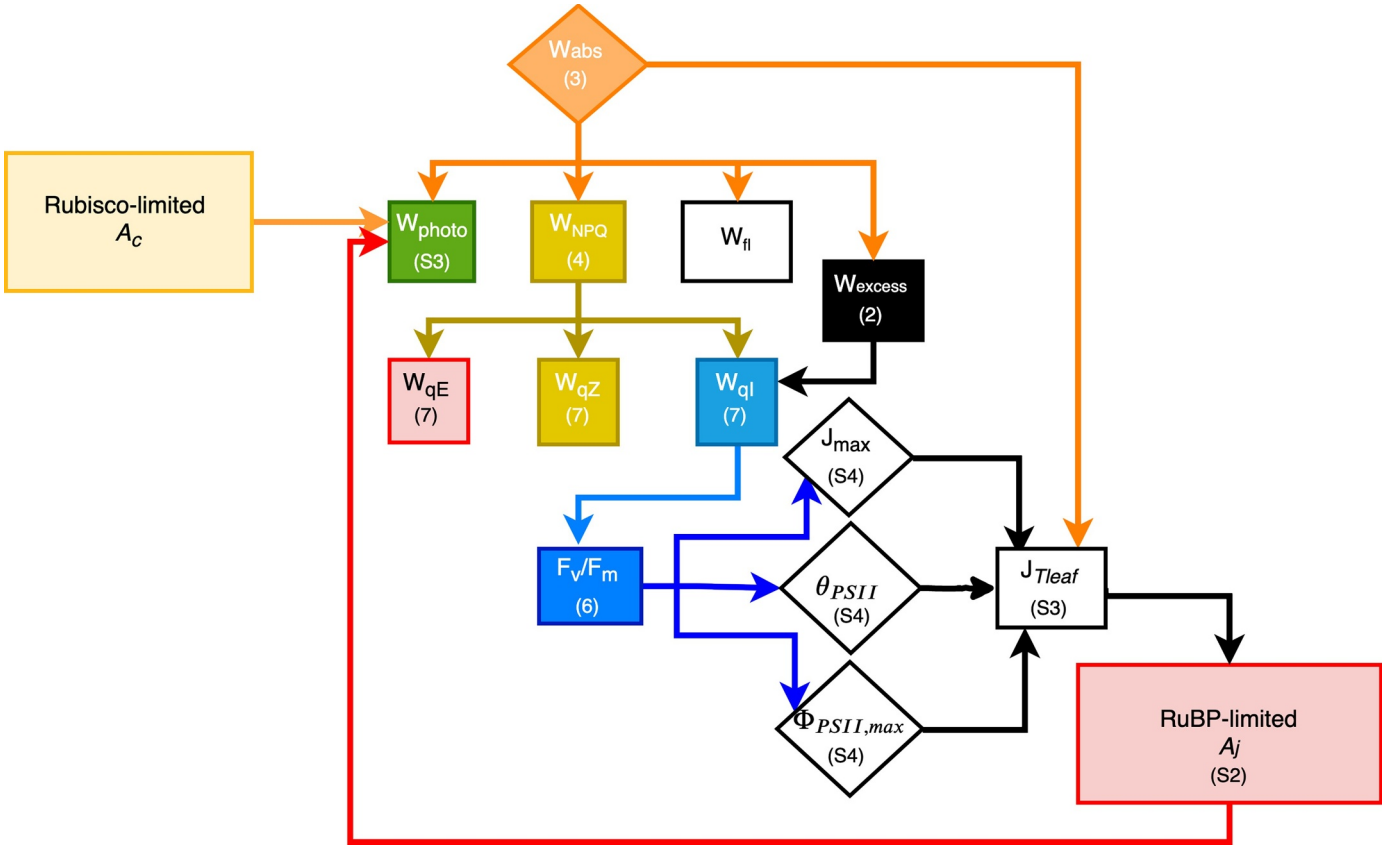

Fig. 1. Diagram illustrating the relationship between the most relevant variables involved in the RuBP-limited dynamic model. Here F_v/F_m serves as the coupling variable to scale FvCB RuBP-regeneration parameters relative to the state of energy dissipation in NPQ. An exhaustive list of all the symbols associated to the variables and parameters is listed in Table S1. Equation numbers are depicted at the bottom of the respective variables and parameters symbols.

diminished photosynthesis; (2) to measure and model photosynthetic and chlorophyll fluorescence responses to water deficits and high temperatures; and (3) to parameterize and test the proposed model to estimate fluxes of absorbed energy to photochemical and non-photochemical quenching.

2. Model theory

The model proposed in this paper adds a dynamic photoinhibition component to the FvCB photosynthesis model. The basis of the FvCB model used in this work is presented in further detail as Supplementary Material. Fig. 1 illustrates a general scheme of the integration of variables and components involved in this model. In this section, we present a more detailed representation for the RuBP-limited processes, which are the focus of this model.

2.1. Linking photoinhibition to Fvcb

In the FvCB model, the irradiance response of RuBP-regeneration is determined by three parameters: the maximum electron transport rate (J_{max}), maximum quantum efficiency of the irradiance response curve ($\Phi_{PSII,max}$), which is related to yield of O_2 evolution, and a curvature parameter (θ_{PSII}). Our model assumes that these FvCB parameters underlying RuBP-regeneration scale in a predictive manner with the maximum photochemical efficiency of PSII in the dark (F_v/F_m) as measured by chlorophyll fluorescence. In the past, linkage functions have been found for F_v/F_m to $\Phi_{PSII,max}$ or quantum yield of O_2 evolution (Björkmann and Demmig, 1987; Demmig et al., 1987; Ogren and Evans, 1992; Werner et al., 2001); and F_v/F_m to θ_{PSII} and J_{max} (Werner et al., 2001). We propose an exponential linkage function, suggested by empirical relationships, to relate irradiance responses to chlorophyll fluorescence parameters (Eqn. 1).

$$Parameter = \delta + \varepsilon \times e^{(\gamma \times F_v/F_m)} \quad (1)$$

where δ, γ and ε are specific for each irradiance response function parameter (i.e. J_{max}, $\Phi_{PSII,max}$ and θ_{PSII}). This relationship could be replaced with others suitable for given data.

Werner et al. (2001) used a similar approach to model photoinhibition and related F_v/F_m to the sum of long-term dose of irradiance. However, exposure to irradiance did not incorporate stress such as limited photosynthetic quenching due to stomatal closure or high temperature. Thus, a key step is to mechanistically link the coupling factor, F_v/F_m, with the responses of PSII to stress. To do so, the input flux of absorbed photons to PSII (W_{abs}) is modeled as the sum of dissipative processes:

$$W_{abs} = W_{photo} + W_{NPQ} + W_{fl} + W_{excess} \quad (2)$$

where each variable (μmol m^{-2} s^{-1} photon equivalent units) is defined in the paragraphs below and in Table S1. The advantage of using this photon-balance equation is that stress and damage can be modeled directly. The components of energy dissipation at PSII already incorporate responses to the environment through the conventional FvCB model: high irradiance through W_{abs}, and high temperature and stomatal closure through effects on photochemistry (W_{photo}). The total absorbed photon flux is calculated according to the relationship (von Caemmerer, 2000):

$$W_{abs} = \alpha \times \beta \times PPFD \quad (3)$$

where α is the leaf absorptance, which was assumed to be 0.85 (Evans, 1987) and β is the portion of absorbed quanta that reaches PSII; assumed to be 0.5 for C3 plants (von Caemmerer, 2000). W_{photo} is a function of photosynthetic fluxes and the flux of energy to

photorespiration, and therefore, it is modeled by the FvCB variable J_{Tleaf} (Eqn S3, the flux of electrons transported through PSII).

W_{NPQ} is considered as consisting of three components of non-photochemical quenching (NPQ) q_E, q_Z and q_I; *sensu* Jahns and Holzwarth (2012): q_E is a very rapid dynamic component of NPQ (time scale < 1 hour), q_Z is a rapid dynamic component of NPQ (time scale < 1 day), and q_I is a slow occurring dynamic component of NPQ that relates to a number of processes that inactivate, damage and affect photochemistry (time scales > 1 day). Here these components are modeled as complementary fluxes summing, such as:

$$W_{NPQ} = W_{qE} + W_{qZ} + W_{qI} \quad (4)$$

Note that q_z and q_I are sometimes combined by researchers (e.g. Horton et al., 2005; Nilkens et al., 2010; Ruban, 2016), and the model developed here does not assign specific biochemistry to these terms, thus the identities of q_Z and q_I fluxes are not set in this model, but relate to NPQ processes empirically derived.

W_{excess} is the residual energy not dissipated by other sinks. Lastly, fluorescence quenching is a quantitatively small component, which is included as a constant fraction for completeness (1% of W_{abs}).

2.2. Dynamic modeling of NPQ

The flux of energy dissipated by NPQ varies over time (W_{NPQ}). Leaves, most of the time, have a greater capacity for NPQ than is actually used ($W_{capacity}$); the capacity increases or decreases based upon the need for dissipation by NPQ ($W_{attractor}$). Thus, the capacity to do NPQ were modeled dynamically by a continuous function of time, such as:

$$W_{x,capacity,t} = W_{x,capacity,t-\Delta t} + \frac{W_{x,attractor} - W_{x,\ capacity,t-\Delta t}}{1 + \tau_x/\Delta t}$$

$$\text{suchthat, } W_{x,capacity,t} \le W_{x,capacity,max}. \quad (5)$$

Here $W_{x,capacity,t}$ represents the generic photons dissipation capacity of x quenching component (i.e. W_{qE}, W_{qZ} or W_{qI}; μmol m^{-2} s^{-1}) at time t based on the previous time (t-Δt), and Δt is the time interval between modeled points. $W_{x,capacity,max}$ represents the maximum capacity for a given x quenching component, which are estimated as described at the end of this section. A time interval (Δt) of 5 min was used; thus, shorter time constants are assumed as instantaneous, while longer time constants (>1 hr) can be resolved and calibrated within the model. Time constants (τ_x) are defined as the time required by each $W_{x,\ capacity}$ to increases or decreases to satisfy NPQ demands. The dynamic equation (Eqn 5) also includes $W_{x,attractor}$ that sets the value that $W_{x,capacity,t}$ is drawn towards. Thus, $W_{x,attractor}$ is the amount of photons required to dissipate by quenching component x at time t. Biochemically, for relatively rapid dynamic components (i.e. W_{qE} and W_{qZ}) the attractor could be related to lumen pH (Müller et al., 2001). Hence, $W_{qE,attractor}$ and $W_{qZ,attractor}$ represent a signal of the state of excess absorbed photons before accounting for the dissipation by NPQ fluxes ($W_{excess,no\ NPQ}$). These attractors can also be defined as the flux of energy necessary for NPQ to absorb in order to avoid excess photons ($W_{excess,\ no-NPQ} = W_{abs} - W_{fl} - W_{photo}$. Alternatively, for the slow component W_{qI}, the attractor is defined as a longer-term signal of excess energy, which it can lead to photoinhibition. Therefore, W_{excess} from the previous time step affects PSII by upregulation of $W_{qI,capacity,}$ and in return, the W_{qI} capacity affects F_v/F_m according to Eqn 6.).

$$F_v/F_m = F_v/F_{m\max} - \frac{W_{qI,capacity,t-\Delta t}}{W_{qI,capacity,\max}} \times F_v/F_{m\max} \quad (6)$$

Here $F_v/F_{m,max}$ (~0.83) is the observed maximum value of F_v/F_m and the slope is determined as the ratio between actual and maximum $W_{qI,capacity}$. Thus, F_v/F_m is modeled as a linear function of the long-term $W_{qI,capacity}$ component of NPQ, such as previously proposed by Jahns and Holzwarth (2012) and Werner et al. (2001). As a result, the photosynthetic flux (W_{photo}) is linked to the dynamics of RuBP-regeneration by a direct link to F_v/F_m changes. An underlying assumption is that at time zero of the model run, there will be no previous photoinhibition effect. Thus, the model should be run for a few time steps (equivalent to 1 hour) to reach equilibrium as a result of a build-up of the three $W_{x,\ capacity,\ t}$.

These equations produce a capacity for NPQ that in some instances will be greater than the excess energy that needs to be dissipated (e.g. in low irradiance). Thus, if $W_{excess,no\ NPQ} < W_{qE,capacity,t} + W_{qZ,capacity,t} + W_{qI,capacity,t}$, then the flux to each NPQ component is apportioned with equal weighting such that the sum is equal to $W_{excess,no\ NPQ}$:

$$W_{x,t} = W_{x,capacity,t} \times \frac{W_{excess,noNPQ,t}}{W_{NPQ,capacity,t}}. \quad (7)$$

If $W_{excess,no\ NPQ,t} \ge W_{NPQ,capacity,t}$ then the W_x is simply the current capacity ($W_{x,capacity,t}$) and at the next time point $W_{qI,capacity,t}$ increase.

In summary, as illustrated by the graphical abstract, this model is based on a dynamic budget of photon dissipation by W_{photo}, $W_{NPQ,}$ and W_{excess}. The long-term NPQ component, $W_{qI,capacity}$ dissipates excess photons over time. Thus, $W_{qI,capacity}$ will depend on the dissipation by other mechanisms by the relationship with F_v/F_m, and vice versa.

3. Material and methods

3.1. Experiment setup

In 2014, the study site was located at the University of California Davis, Plant Sciences Experimental Orchard using fully grown almond trees (cv. Nonpareil). Daily maximum temperatures spanned 20.1 to 41.1 °C for the May to September experimental period. Trees were spaced 5.5 × 3.5 m apart and were irrigated by micro-jet sprinklers. Two orchard rows were divided into thirds and each third received one of three water stress treatments (Table S2). Four trees were randomly selected from each stress treatment to collect midday stem water potential (Ψ_{st}), stomatal conductance (g_s), and gas exchange measurements. Three single leaves near the trunk were collected, twice a week, from each tree, to perform stem water potential measurements with a Scholander pressure chamber (PMS Instruments Inc). Leaves were covered with an opaque foil bag for 45 min prior to excision. Midday leaf stomatal conductance was also measured on the same day as stem water potential observations. Soil water content at 30 cm was monitored and individual sprinklers were turned off when necessary to maintain the soil water content of the three treatments in defined ranges (Table S2).

The second study site in 2015 was a field at Orchard Park, UC Davis, where sixteen potted 4-year-old almond trees (cv. Nonpareil, in 56 L pots) were placed to facilitate measurement under extreme stress conditions (i.e. heat and drought), which were necessary for a broad parameterization of the model. Half of the trees were well-watered (CT; control) and the other half were severely stressed (SS, severe stress). Stem water potentials were measured until a level of stress was reached that was equivalent to field observations for both CT and SS treatments. Throughout the experimental period the daily maximum temperature ranged from 19.4 to 50.6 °C. Particularly hot temperatures were probably due to a nearby building, which provided additional radiative forcing and diminished wind.

3.2. FvCB model parameterization

Photosynthesis and stomatal measurements were performed using a LI-6400XT System with either a 6400–02B leaf chamber (6 cm^2) or a 6400–40 fluorometer chamber (2 cm^2 leaf area) (LI-COR, Inc., Lincoln, NE, USA). Leaves were acclimated to either sun exposed or shaded conditions by placing fine metal meshes ~20 cm above some leaves for

periods of more than a week. A quantum sensor (LI-190R, LI-COR, Inc) was used to measure an average midday PPFD, which was in the range of 500 to 800 μmol photons $m^{-2} s^{-1}$ for leaves under a mesh and 1200 to 2000 μmol photons $m^{-2} s^{-1}$ for leaves under direct sun.

A_n values for intercellular CO_2 curves (A_n/C_i) were measured at CO_2 concentrations ranging from 50 to 2000 μmol CO_2 mol^{-1} air. At least three A_n/C_i curves were performed on both sunny and shaded leaves at optimum conditions, which were defined by three criteria: 1) $F_v/F_m \geq 0.80$, 2) $\Psi_{st} \geq -1.0$ MPa, and 3) $g_s \geq 150$ mmol $m^{-2} s^{-1}$. A_n/C_i curves were measured over a range of T_{leaf} from 17.5 to 45 °C with increments of ~ 2.5 °C for the pot experiment.

Photosynthetic irradiance-responses (A_n/PPFD) were measured in the range 0 to 2000 μmol $m^{-2} s^{-1}$ PPFD and within a range of T_{leaf} from 17.5 to 45 °C with increments of ~ 2.5 °C. At least three A_n/PPFD curves were measured on both sunny and shaded leaves under non-stress conditions. Additionally, a total of 14 curves were measured on leaves with different levels of stress and/or damage according to values of F_v/F_m. These measurements were performed at a constant chamber temperature of 35 °C and either a constant C_a of 420 μmol CO_2 mol^{-1} air or a constant C_i of 250 μmol CO_2 mol^{-1} air in cases of severe water stress to avoid stomatal closure effects on the A_n/PPFD response.

3.3. Dynamic model parameterization: chlorophyll fluorescence

The ratio F_v/F_m represents the maximum efficiency of PSII under dark adapted conditions (Baker, 2008). During the day, only the actual quantum yield of PSII (Φ_{PSII}) photochemistry can be monitored, and this is interpreted as the fraction of absorbed photons that result in photochemistry (Genty et al., 1989). F_v/F_m and Φ_{PSII} were monitored by using a Walz MONI-PAM fluorometer, which is widely used in stress research (e.g. Aalto et al., 2015; Meacham et al., 2016; Webster et al., 2016). Four fluorometer emitter-detector units with PPFD sensors (MONI-head/485) were deployed for the experiments in both field and potted almond trees. In the field, construction scaffolds allowed fluorometers to be installed in the upper canopy. A fine gage K-type thermocouple was sprung to press against the underside of each leaf. Four leaves were continuously measured for a period of ~ 7 days with factorial treatments: 1) severe water-stress and shaded, 2) severe water-stress and sunny, 3) control and shaded, and 4) control and sunny. The MONI-PAM was programmed to execute a daily set of measurements (Table S3). Irradiance responses were performed by the MONI-PAM over an hour period before dawn, starting with a measurement of F_v/F_m then increasing PPFD from 0 to 1600 μmol $m^{-2} s^{-1}$ using actinic light from the MONI-PAM system.

To complement the assessment of model performance, the MONI-PAM system was used to collect measurements of F_v/F_m on dark-adapted leaves during the daytime. This was achieved by placing the fluorometer and leaf in the dark for 20 min, in a mylar envelope covered with black felt and Reflectix aluminized insulation to minimize temperature increases.

3.4. Temperature responses

Photosynthesis parameters for the FvCB model (i.e., V_{cmax}, g_m, and J_{max}) were fit to data from field measurements. The curve-fitting method of Sharkey et al. (2007) was used to fit seven A_n/C_i curves in the range of ~17.5 to ~43.5 °C. Note that the Sharkey et al. (2007) method was only used to parameterize the Rubisco-limitations within the FvCB model, and was not used to parameterize the RuBP-regeneration components related to irradiance responses; thus the results are largely independent of the performance of the A_n/C_i curve modeling. Based on these A_n/C_i curves, an approximate g_m response to temperature was calculated and used to derive C_c for the remaining curves. Following this method, 93 A_n/C_c curves were used to estimate V_{cmax}. V_{cmax} at 25 °C was used to normalize the value of V_{cmax} measured on the same leaf at different temperatures. This combined approach was used to account for finite mesophyll conductance.

J_{max}, θ_{PSII} and $\Phi_{PSII,max}$ (Eqn 3) were estimated by fitting measurements of absorbed PPFD to electron transport rates from irradiance response curves measured by both the MONI-PAM Fluorometer and the LI-6400XT system. Temperature sensitivity of g_m, V_{cmax}, J_{max}, θ_{PSII} and $\Phi_{PSII,max}$ were modeled by fitting temperature response curves using the Arrhenius function (Eqn S4) or a second order polynomial function (Eqn S5). Non-linear fits were performed solving a nonlinear least-square constrained optimization by a modification of a Levenberg-Marquardt algorithm implemented in *R* (R_Development_Core_Team, 2010).

3.5. Photosynthetic irradiance-response parameters and F_v/F_m relationships

An exponential function (Eqn 1) was used to fit δ, γ and ε to represent the relationship for each irradiance response parameter (i.e. J_{max}, θ_{PSII} and $\Phi_{PSII,max}$) versus F_v/F_m. A total of 238 irradiance response curves collected by the MONI-PAM were used for this parameterization. Additionally, average modeled curves from this parameterization were compared to the previously mentioned 14 photosynthetic irradiance-response curves collected with the LI-6400XT on leaves with different levels of stress; serving as confirmation of the function of the Walz MONI-PAM fluorometer.

3.6. Time constants (τ_x) and maximum Npq capacities ($W_{x,capacity,max}$) optimization

The dynamic nature of our model is based on the optimization of Φ_{PSII} (day) - F_v/F_m (night) time-series. Time constants and maximum NPQ capacities were estimated by performing a bounded optimization using the "*fmincon*" algorithm in MATLAB (R2015b, The MathWorks, Inc., Natick, MA, USA). The sum of the squared difference between time-series of observed and modeled F_v/F_m in the dark (PPFD = 0 μmol $m^{-2} s^{-1}$) as well as observed and modeled Φ_{PSII} under irradiance (PPFD > 0 μmol $m^{-2} s^{-1}$) was minimized. Fits for time constants were bounded based on the assumption of fast (0 to 5 min), intermediate (10 min to 24 hr), and slow (8 hr to 7 days) constants for the q_E, q_Z and q_I NPQ components, respectively (Jahns and Holzwarth, 2012). Maximum NPQ capacities ($W_{x,capacity,max}$) were bounded based upon those reported by Roháček (2010), while minimums were set to be greater than zero.

The optimization procedure for τ_x and $W_{x,capacity,max}$ was performed using eight independent time-series, 7 days long, of measured Φ_{PSII} (day) and F_v/F_m (night). Model outputs from five validation runs, performed by using mean values from calibration for each parameter (Table 2), were compared to corresponding measured Φ_{PSII} and F_v/F_m. W_{photo} was calculated from the FvCB model and thus RuBP-regeneration limited photosynthesis was constrained by responses to the environment. These validation runs were fully coupled to the FvCB model and did not use fluorescence data as a source of information.

3.7. Model evaluation

The proposed model was evaluated in two manners, either as a *coupled model* of our dynamic RuBP-regeneration limited photosynthesis scheme along with the steady-state FvCB model (coupled damage model; DM) as described above, or only as the RuBP-regeneration limited photosynthesis approach (*dynamic model*) solely based on the components of W_{abs} (Eqn 3), with Φ_{PSII} and PPFD as inputs and F_v/F_m as output (damage model with only fluorescence; DMF). For the latter, the electron transport rate through PSII must be estimated by fluorescence observations of quantum yield of PSII (Φ_{PSII}) based on the classical relationship of Genty et al. (1989):

$$W_{photo} = W_{abs} \times \Phi_{PSII} \quad (8)$$

To highlight the relevance of this model, the results are also compared to the steady-state FvCB approach without the dynamic linkage

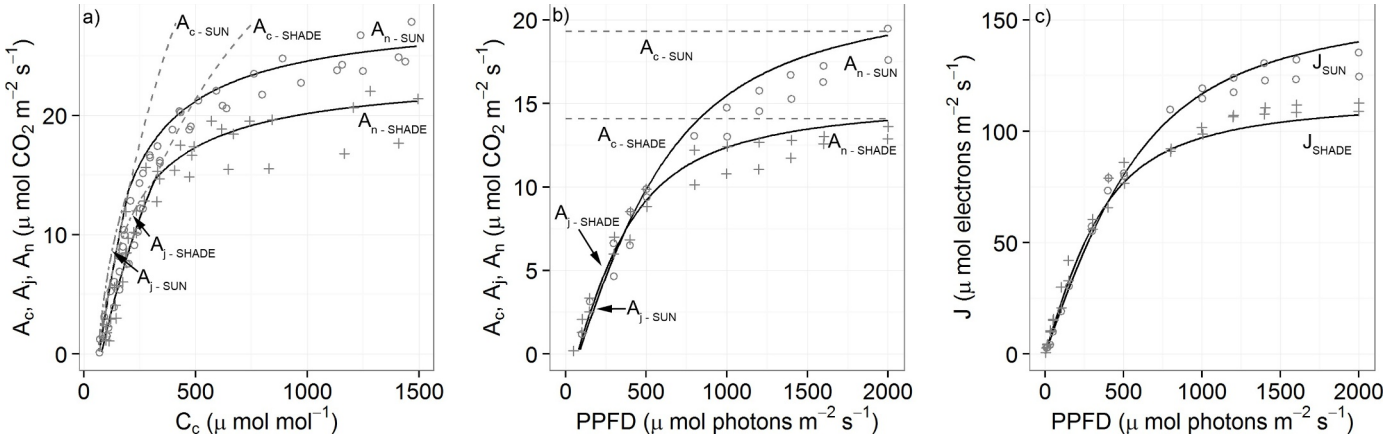

Fig. 2. Measured net photosynthesis or electron transport data for leaves acclimated to sun (o) or shade (+) and the predicted values for the FvCB model for 25 °C, varying CO_2 or PPFD. The predicted model is from fits to broad datasets for A_n/C_c, A_n/PPFD and J/PPFD responses where temperature was varied. Measured A_n/C_c response curves for 25 °C and PPFD of 1500 μmol $m^{-2} s^{-1}$. curves represent modeled Rubisco and RuBP-regeneration limited photosynthesis using the FvCB model (panel a). A_n/PPFD and J/PPFD response curves were modeled at 25 °C, constant g_s of 0.15 mol $m^{-2} s^{-1}$ and 420 μ mol^{-1} ambient CO_2 (panel b and c).

to fluorescence parameters; referred to as "no damage" (ND) in the following sections.

In addition, the DM performance was assessed by comparing model outputs of F_v/F_m during the day-time to observations of dark-adapted leaves in a range of different levels of stress (i.e. ~0.4 < F_v/F_m < ~0.83).

4. Results

The FvCB model was calibrated for almond with A_n/C_c curves and temperature response functions across a broad range of conditions. The predicted C_c response for a leaf temperature of 25 °C is shown for shade and sun acclimated leaves (Fig 2a, fitted parameters: Table S4). A_n/PPFD curves are shown for the fitted values of θ_{PSII} and $\Phi_{PSII,max}$ (Fig 2b). J_{max} was determined by fitting the J/PPFD observed curves (Fig 2c) to a nonrectangular hyperbolic function (Eqn S3). As a validation for these parameter calibrations, the curves are depicted along with two sets of independent observations measured at T_{leaf} of 25 °C. Leaves showed acclimation responses, as strong correlations were found between the average irradiance environment and photosynthesis parameters such as J_{max}, $\Phi_{PSII,max}$ and V_{cmax} (Fig 3), but θ_{PSII} showed little variation. The acclimation represented non-stressed responses as all leaves had sustained F_v/F_m values of about 0.81. In further calibration analyses, J_{max}, $\Phi_{PSII,max}$ and V_{cmax} were adjusted to a standard irradiance environment of 1500 μmol $m^{-2} s^{-1}$ by accounting for irradiance acclimation with the equations presented in Fig 3. Photosynthetic parameters did not appear to acclimate to previous temperature exposure (Fig S2).

4.1. Effect of leaf temperature on FvCB photosynthesis parameters

V_{cmax} and g_m temperature responses showed the well described Arrhenius deactivation shape (Fig 4), similar to responses measured on almonds elsewhere (e.g. Egea et al., 2011). Validation data points were comparable to the calibrated response, for leaves fully exposed to the sun as well as shaded leaves. Irradiance response parameters were also sensitive to temperature, with J_{max} showing an Arrhenius deactivation type response (Fig 4; Table S4) and with θ_{PSII} and $\Phi_{PSII,max}$ characterized by a third order polynomial relationship (Fig 4; Table S4).

4.2. F_v/F_m is an effective variable to scale RuBP-regeneration limited photosynthesis parameters

Significant relationships were found between irradiance response parameters and the fluorescence variable F_v/F_m (Fig. 5, Table 1). The strong relationship between F_v/F_m and J_{max} indicates that photoinhibition would affect A_n under a broad range of irradiances. These results indicate that F_v/F_m can be used as a coupling factor between the degree of photoinhibition and predicting J_{max}, θ_{PSII} and $\Phi_{PSII,max}$ at 25 °C using an empirical exponential relationship (Eqn 1). Acclimation to irradiance environment had an effect on the light response curve parameters to F_v/F_m relationships. This effect can be accounted for by using the observed unstressed acclimation relationships (Fig. 3) to adjust the values of the three light response curve parameters (Fig. 5).

4.3. A dynamic approach is key to accurately represent photosynthetic regulation

After the dynamic damage model (DM) was fit to the calibration data, the time constant of each quenching component (τ_{qI}, τ_{qE}, τ_{qZ}) was remarkably different between upregulation of NPQ mechanisms and the recovery time from NPQ dissipation. For example, we noticed that decreases in F_v/F_m, as controlled by increasing $W_{qI,capacity}$, occurred in hours while F_v/F_m recovery took days (Fig 6 and Fig S3). Fitted τ_x and $W_{x,capacity,max}$ were relatively consistent among the eight different calibration runs resulting in a low standard deviation, and a CV of 8 to 18% (Table 2). Using the calibration values to predict observed data resulted in the final output successfully predicting observed F_v/F_m (Fig 6a, Fig S3). For instance, the rapid upregulation of modeled $W_{qI,capacity}$ (hours) and its negative effect on F_v/F_m (48% decrease) was followed by a slow decrease in $W_{qI,capacity}$ as reflected in the slow recovery of F_v/F_m (Fig 6b, Fig S3). Fig. 6 also illustrates that the model successfully represented physiological responses when analyzing a case of extreme heat and water stress; high air temperatures of above 50 °C within 2 m of the ground on the first day (Sept. 10, 2015) along with below average midday stem water potentials (Fig 6d). In this case, the day of greatest stress had Φ_{PSII}'s lower than 0.05 indicating severe stomatal closure and photosynthetic impairment. This led to rapid upregulation of $W_{qE,capacity}$ in the model, but reached a maximum dissipation rate, followed by a slower induction of $W_{qI,capacity}$ and $W_{qZ,capacity}$. W_{qZ} accounted for little NPQ flux due to a small capacity and slow induction (Table 2). The NPQ components and photochemistry failed to dissipate the excess absorbed PPFD (Fig 6b). In the DMF mode, the excess photons lead to an increase in W_{qI} capacity which decreases F_v/F_m (Eqn 6).

Small standard deviations on the recovery parameter values (Table 2) indicate that variation in irradiance and temperature regimes between experiments resulted in little variation in recovery rates. The $\tau_{qI,decrease}$ time constant was ~45 h and so typically a considerable recovery was observed a few days following a major stress event.

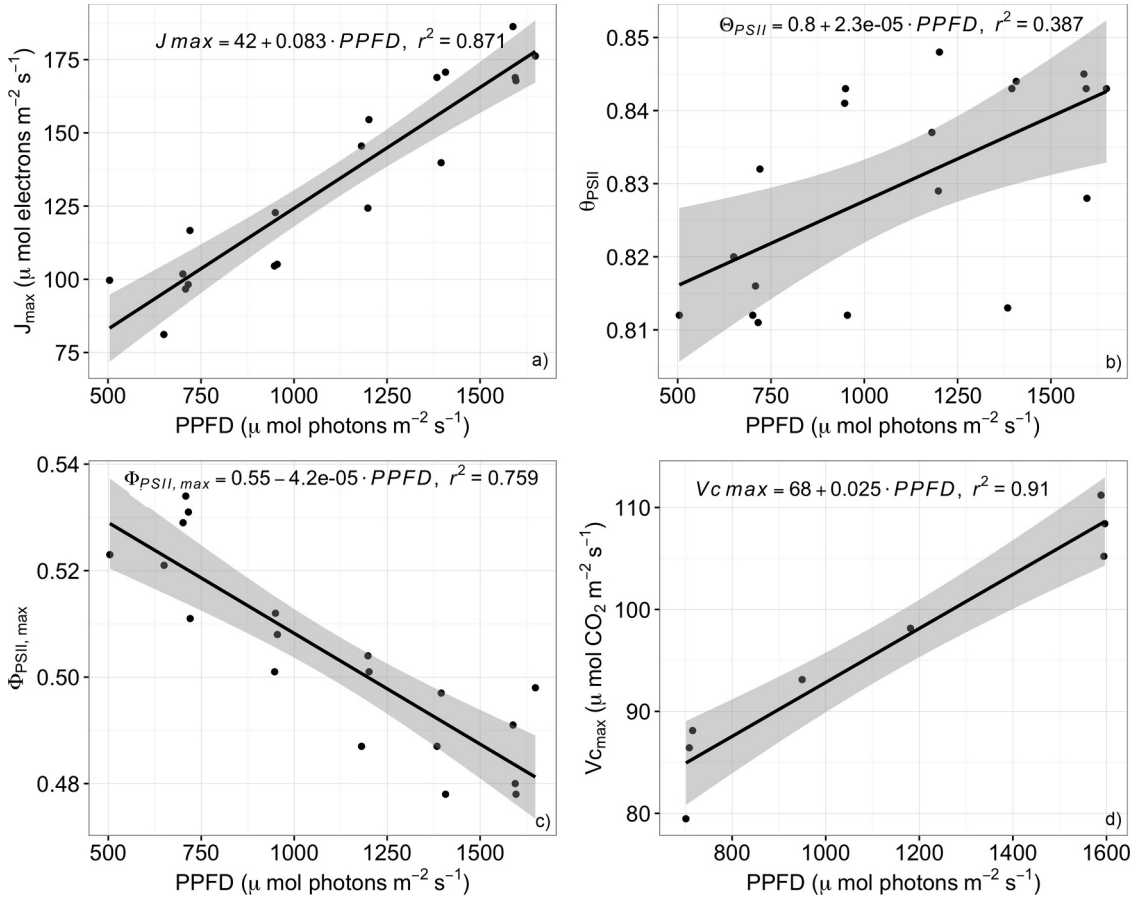

Fig. 3. Photosynthetic parameters, J_{max}, $\Phi_{PSII,max}$, θ_{PSII} and V_{cmax}, relative to the average PPFD to which the leaves were acclimated (PPFD averaged from 12 to 4pm for five days prior to measurement). Linear fits are shown, with confidence interval of the fit.

4.4. Day F_v/F_m measurements on dark adapted leaves confirm the predictability of a dynamic approach

Model performance was assessed by comparing observed F_v/F_m from independent time-series to the F_v/F_m outputs from the calibrated dynamic version of the coupled damage model (DM). A broad range of conditions were evaluated, with four different combinations of treatments (i.e. irradiance and water stress) over 20 days and at four different times of day; two F_v/F_m values per treatment measured at night and two measured via dark adaptation during the day. The model accurately estimated F_v/F_m under a wide range of environmental stressors such as high temperature, water deficit, as well as photoinhibition ($\sim 0.4 < F_v/F_m < 0.82$) (Fig 7). Note that the model was not calibrated by using observations of F_v/F_m on dark-adapted leaves during the daytime, and its ability to predict these values could be considered as a good independent test of model performance.

4.5. FvCB model might not accurately represent photosynthetic dynamics under stress

A validation exercise of the model was performed running the model in three different modes (Fig 1), the fully coupled dynamic and FvCB model (DM), dynamic model only with fluorescence inputs (DMF) and the no-damage FvCB model (ND). The period of data is based on observations for the same period presented for the model calibration, but in these model runs, the NPQ components and time constants were represented by the mean values obtained from all the calibration runs (Table 2). Runs in DM mode functioned well across broad environmental ranges. The results for net photosynthesis clearly show the importance of explicitly representing the effect of stress and photoinhibition (DM versus ND; Fig 8). The FvCB (ND) model overestimated photosynthesis when plants are exposed to stress compared to those estimations from model runs in both DM and DMF modes. Observed and modeled Φ_{PSII} or F_v/F_m based upon the damage model (DM) are comparable. However, DM seems to slightly overestimate Φ_{PSII} relative to observations under scenarios of high stress.

5. Discussion

5.1. Insights from integrating chlorophyll fluorescence and gas exchange measurements

Here the standard steady-state FvCB model of photosynthesis was calibrated and coupled to an additional dynamic model that accounted for photoinhibition and photosynthetic stress. This new approach was able to capture the dynamics of photoinhibition and recovery for periods of up to a week, and semi-mechanistically coupled stress effects with photoinhibition e.g. stomatal closure, high temperature, high irradiance. F_v/F_m was an effective coupling factor for the three FvCB irradiance response parameters when perturbed by a combination of stressors (Fig. 5). Such relationships, particularly for $\Phi_{PSII,max}$, may be general as similar responses have been found for a broad array of species (e.g. Long et al., 1994; Öquist et al., 1992; van der Tol et al., 2009), although between species differences deserve more attention. The response of J_{max} to F_v/F_m is less well described, and it would be key to further investigate the relationship found in this work.

Uniquely, the dynamic model incorporates acclimation to irradiance and stress environment through the adjustment of the capacities for NPQ (1 min to ~7 days), and accounts for acclimation effects of irradiance environment on FvCB photosynthetic parameters. The structure

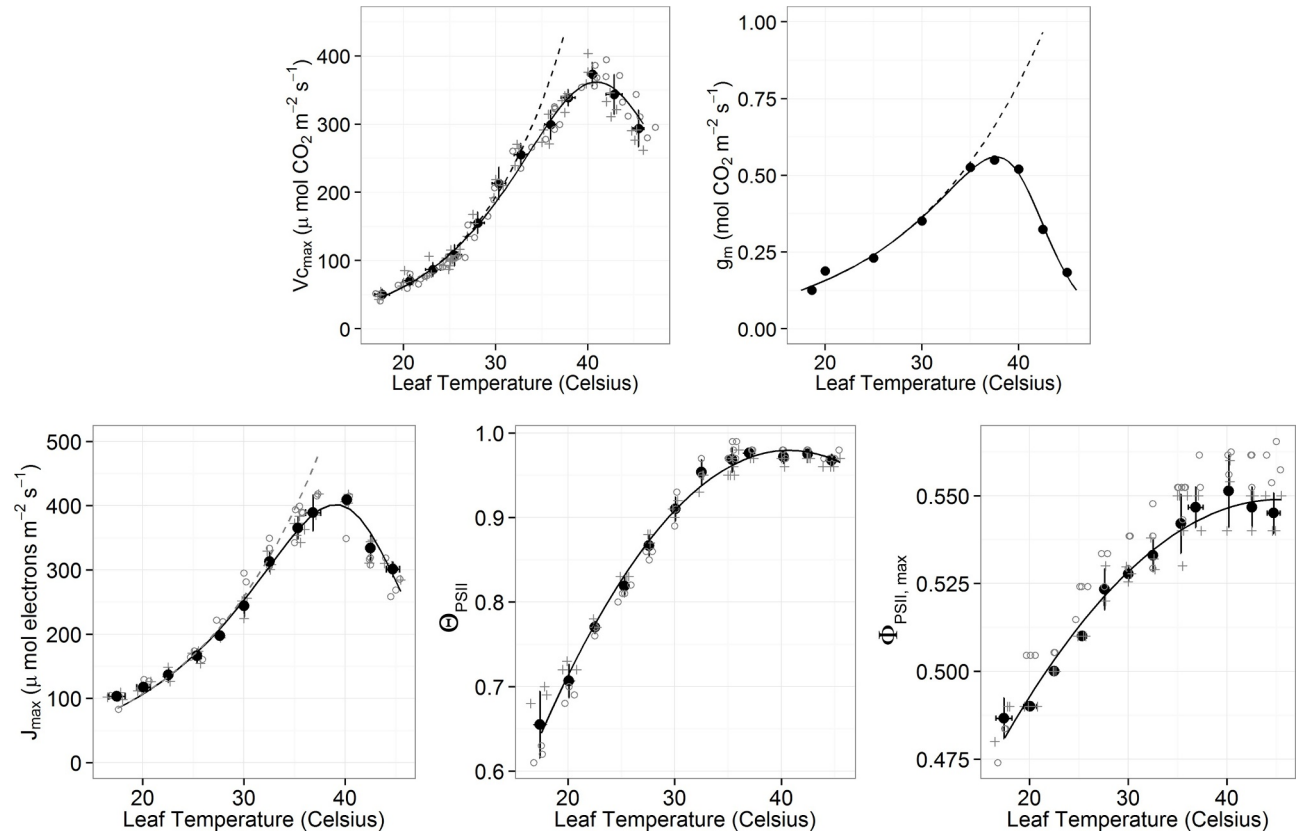

Fig. 4. Temperature responses of five parameters from the FvCB model determined from gas exchange and chlorophyll fluorescence observations on almond trees. Curves were fit to mean values of observations within a range of +/- 0.75 °C, which are represented by black filled circles and +/- 1 standard error. Observations used to calculate these mean values are presented by (o) and (+) for measurements collected on leaves acclimated to full sun or shade, respectively. All parameter values were standardized for an irradiance environment of 1500 μmol $m^{-2} s^{-1}$ using the equations presented in Fig 3.

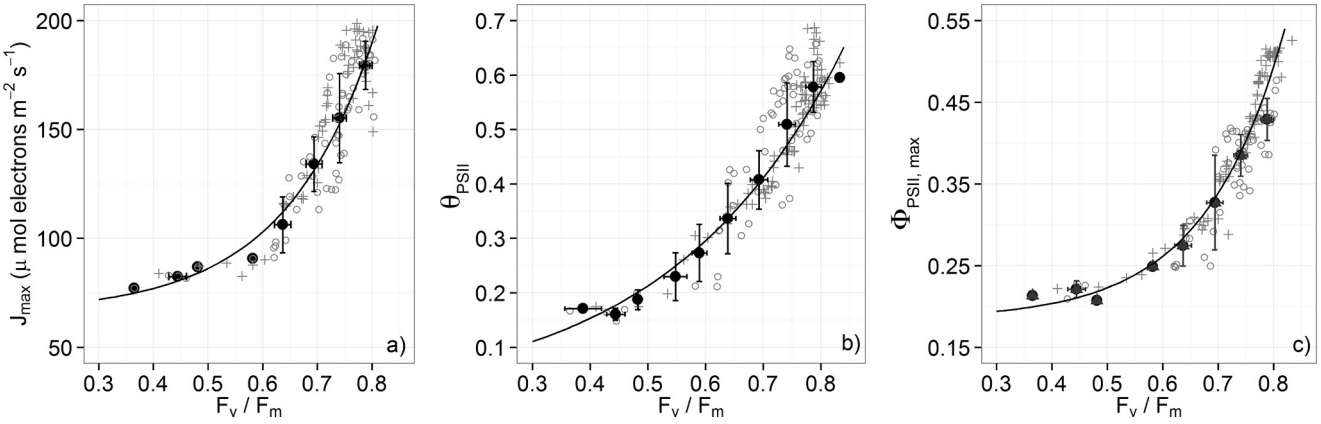

Fig. 5. RuBP-regeneration parameters response to F_v/F_m. Curves were fit to mean values of F_v/F_m observations within a range of +/- 0.05, which are represented by black filled circles and the +/- 1 standard error. Observations used to calculate mean values are presented by (o) and (+) for measurements collected on leaves acclimated to full sun or shade, respectively. All parameter values were standardized for an irradiance environment of 1500 μmol $m^{-2} s^{-1}$ using the equations presented in Fig 3.

Table 1
Parameters to represent irradiance response curve response to F_v/F_m.

	δ[1]	ε	γ
$J_{max@25}$	31.84	1.11e-02	12.18
$\Phi_{PSII,\ mx@25}$	1.84e-01	1.19e-03	6.96
$\theta_{PSII@25}$	–	4.15e-02	3.29

[1] The regression coefficients were significant at $P < 0.0001$ for all parameters with exception of ε for $\Phi_{PSII,max}$, in which case the regression coefficient was significant only at $P < 0.1$.

of the dynamic model would function generally for any irradiance related photosynthetic stress as this would lead to decreases in W_{photo} and excess absorbed photons and thus photoinhibition. For instance, the current model may be applicable under conditions were photosynthesis is limited by photoinhibition under cold temperatures (e.g. Öquist and Huner, 2003). In the past, models were limited to empirically linking water potential, high temperature or cumulative irradiance dose to photosynthesis parameters. For instance, if photoinhibition was modeled based on a cumulative irradiance dose, then shaded plants would always have less photoinhibition. However, shaded plants can have

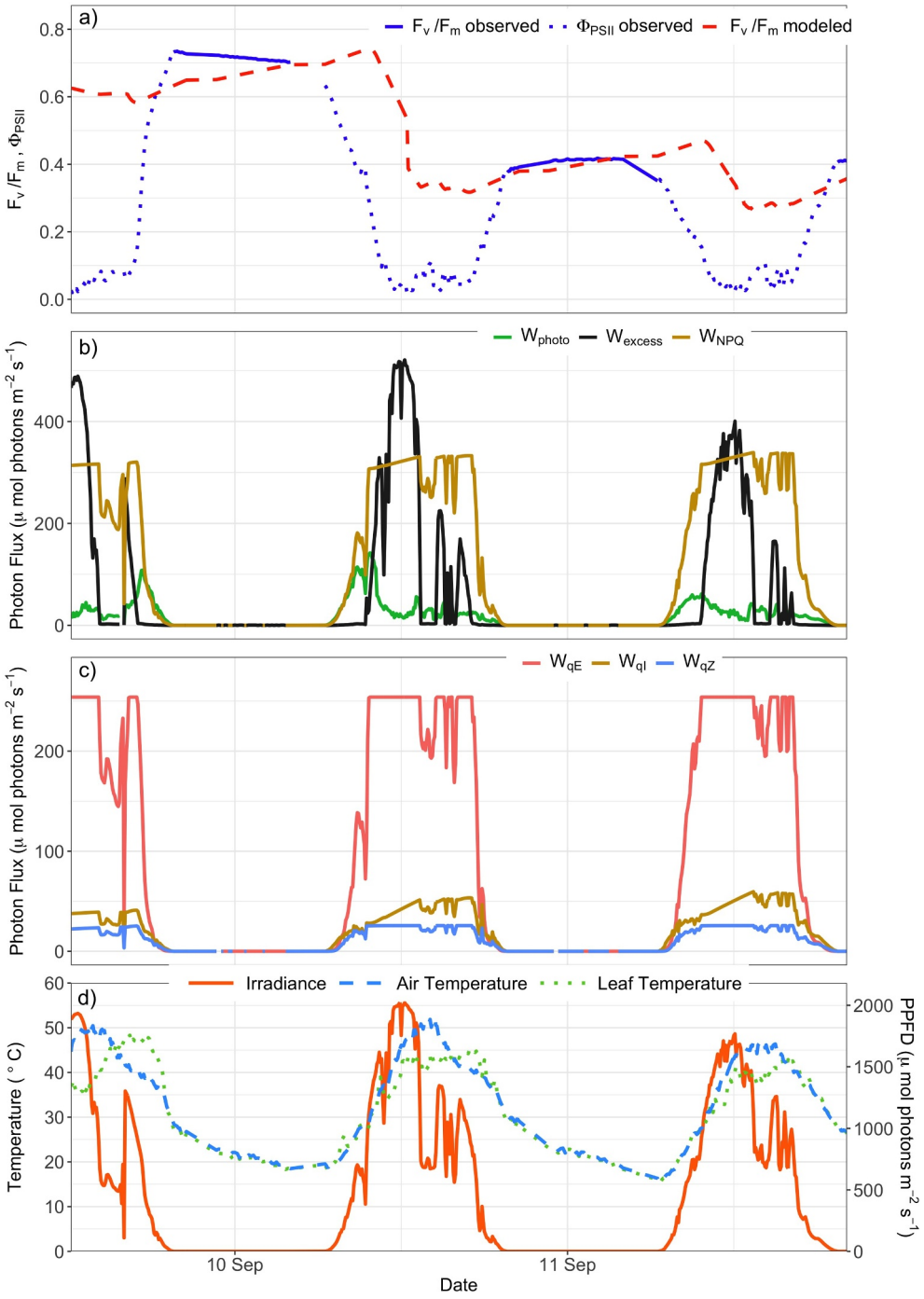

Fig. 6. Dynamics of observed and modeled (DM) chlorophyll fluorescence parameters and NPQ mechanisms through three days of high irradiance intensity, high temperatures, and drought. Observed F_v/F_m and Φ_{PSII} along with F_v/F_m estimations from the DMF dynamic model are shown (a), modeled dissipation of photons by photochemistry and the sum of NPQ mechanisms and excess of photons (b), NPQ mechanisms (W_{qI}, W_{qE}, and W_{qZ}) (c), and irradiance, air and leaf temperature time series (d). An extended time period from of this dataset is shown in Fig S3.

greater photoinhibition than plants fully exposed to the sun due to larger constraints on photochemical quenching of excess absorbed irradiance (Valladares and Pearcy, 2002). Our model uses a budget of excess absorbed irradiance to link the effects of stresses, and thus provided photosynthesis parameters were adjusted for irradiance acclimation, and shade leaves could be modeled to have greater photoinhibition. Moreover, longer acclimation responses could be studied within this model scheme.

5.2. NPQ should be accounted to understand long-term plant responses to environmental stress

Plants have developed photoprotective mechanisms to minimize inhibition and potential damage from excessive photon flux. Heat dissipation, fluorescence emission and state transition are some of those mechanisms, which are well represented by non-photochemical quenching (NPQ) of excitation energy in PSII (Goh et al., 2012;

Table 2
Mean and standard deviation of NPQ parameters from optimization runs .

Parameter	Mean	SD	Units
$W_{qE,capacity,max}$	262.3	21.5	μmol $m^{-2} s^{-1}$
$\tau_{qE}^{increase}$ [1]	1.7	0.3	min
$\tau_{qE}^{decrease}$	5.3	0.2	min
$W_{qZ,\ capacity,max}$	24.7	2.3	μmol $m^{-2} s^{-1}$
$\tau_{qZ}^{increase}$	53.4	5.5	min
$\tau_{qZ}^{decrease}$	115.5	11.9	min
$W_{qI,\ capacity,max}$	223.7	31.6	μmol $m^{-2} s^{-1}$
$\tau_{qI}^{increase}$	70.2	10.3	min
$\tau_{qI}^{decrease}$	2709.3	202.1	min

[1] "increase" represents the time constant for an upregulation of a $W_{x,capacity}$ term, "decrease" is vice versa.

Ivanov et al., 2008; Ye et al., 2013). Our model accounts for potential damage affecting those photoprotective mechanisms, and our results demonstrate how this could be relevant on occasions when plants face water deficit and high temperatures. The fast NPQ component, W_{qE}, was quantitatively the most important mechanism minimizing excess absorbed energy (Fig 6b, Table 4). This fast upregulation of photon dissipation is associated with a decrease in pH within the thylakoid lumen, which is an immediate signal of excessive irradiance that triggers the feedback regulation of irradiance harvesting by W_{qE} (Müller et al., 2001). The control by lumen pH allows induction or reversal of q_E within seconds of a change in irradiance intensity, which is fast enough to cope with natural fluctuations in irradiance intensity. $W_{qZ,capacity}$ relaxes within minutes but is considered the least important photoprotection mechanism in plants (Niyogi, 1999), yet it can have a significant impact on yield over time (Kromdijk et al., 2016). Based on our results, q_Z would represent about 5% of the total NPQ dissipation. This component is due to the phenomenon of state transition, when the major irradiance-harvesting complex separates from PSII, thus reducing the amount of excitation energy in PSII. Finally, W_{qI} was an important photoprotective mechanism and accounted for the long-term dynamics in F_v/F_m and photosynthetic parameters. This NPQ mechanism is much less characterized and might be due to a mix of photoprotection and photodamage. Previously, it has been proposed that this mechanism would occur within minutes to hours (Müller et al., 2001; Roháček, 2010), but relax over longer periods. Here, W_{qI} had fast induction (69 min), and slow relaxation of about 45 h, contributing to a considerable dynamic photoinhibition limitation to net photosynthesis.

Our results are comparable to fluorescence dynamics found in M. species such as *Eucalyptus* (Correia et al., 2014; Ogren and Evans, 1992), grapevines (Luo et al., 2011), *Zea mays* (Virlouvet et al., 2018), and *Calotropis procera* (Rivas et al., 2017). However, in cases when plants are exposed to consistent stress, photoinhibition could persist. These results are difficult to compare to other studies since long-term photosynthetic responses to stress have been poorly studied, and there were limited techniques to monitor in vivo photosynthetic responses, at field scale, and throughout long periods of time. It should be noted, that the NPQ fluxes were assigned using a numerical solver based on the fluorescence transients, and therefore the identities of the fluxes may not correspond directly to the NPQ fluxes as defined elsewhere in the literature.

5.3. Does photoinhibition limit photosynthesis quantitatively?

Photoinhibition is the irradiance dependent and slowly reversible retardation of photosynthesis, which translates into a decrease of $\Phi_{PSII,max}$ and O_2 evolution, as well as a reduction in θ_{PSII} (Long et al., 1994). Here it is found that a long exposure to excessive irradiance also leads to impairment of J_{max} – which would be associated with decreased photosynthesis under high irradiance fluxes. The current results show that photoprotective mechanisms operate from seconds to weeks, and consequently, recovery takes place during that time scale as well. These results strongly support the necessity of including the effect of stress on photosynthesis due to photoinhibition in plant models, especially considering climate change trends. These results might seem discordant with the small reduction of CO_2 uptake due to photoinhibition estimated at the canopy level (Long et al., 1994; Werner et al., 2001). However, when comparing leaves from well-watered plants throughout a regular day in terms of temperature, our results are similar. Under those environmental conditions, based upon simulations in DM mode, it was found that photoinhibition can impact CO_2 uptake from 2 to 10%, and these effects did not last longer than a day in most cases. However, the experimental conditions used in the current experiments are similar to environments that plants routinely experience in natural or agricultural landscapes: full sun, severe stomatal closure due to soil water

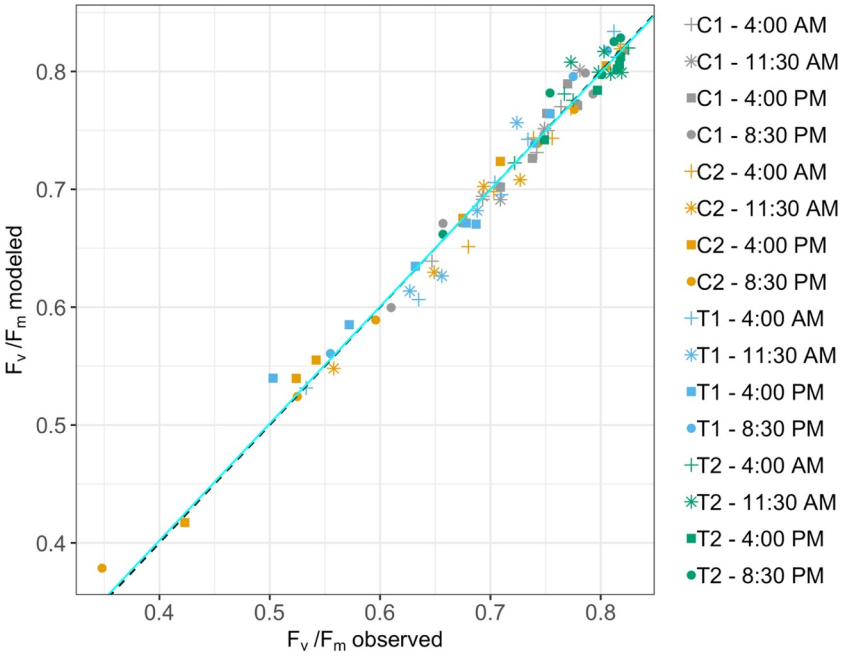

Fig. 7. Comparison between observed and modeled F_v/F_m from the dynamic model (DM). These data represent a wide range of environmental conditions and water stress treatments. The DM was run for observations of PPFD and T_{leaf}, while F_v/F_m observed was collected on control (C1 and C2) and severe water stress treatment (T1 and T2) plants. Daylight observations of F_v/F_m were measured on dark-adapted leaves. The solid line represents a fitted linear relationship (Intercept = 0.004907, Slope = 0.9928, R^2 = 0.98, $P < 0.0001$, n = 84), and the dashed line represents a 1:1 relationship.

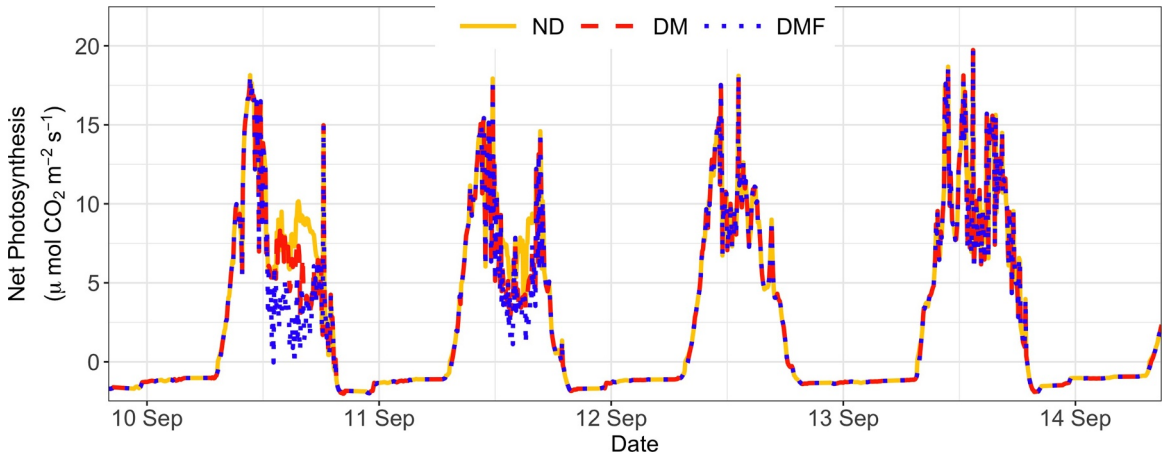

Fig. 8. Dynamics of net photosynthesis modeled using three different approaches: the FvCB model (no damage; ND), the new dynamic photosynthesis model coupled with the FvCB model (damage model; DM), and the dynamic model with Φ_{PSII} observations as input (damage model with fluorescence; DMF). The period illustrated corresponds to an extended period of results presented in Fig 6; characterized by high irradiance intensity, extremely high temperature, and water stress (plants were irrigated on the evening of September 11th).

deficit and hot leaves due to high air temperatures. The current model incorporates feedbacks and thus would lead to increasing photoinhibition with time, whereas past models would be conservative as photoinhibition is modeled as unrelated to dissipative fluxes. For example, in our dynamic model: photoinhibition leads to low photosynthesis, thus the resulting lower dissipation of energy leads to a negative feedback of more photoinhibition. Consequently, for many plants large photoinhibitory decreases in net photosynthesis are expected (Flexas and Medrano, 2002). RuBP-regeneration is an important limitation to photosynthesis in canopies, as the majority of leaves receive lower light than saturating. Thus, a model of RuBP-regeneration limitation is likely to be important in many environments, and for productivity of both natural and agricultural systems.

5.4. Advantages and disadvantages of a dynamic model of photosynthetic responses to irradiance, heat and water stress

Plants have “memory” and responses to stress at a given time seem to depend on previous exposure to a given environmental stressor Virlouvet et al., 2018). Our dynamic approach builds on the widely used steady-state FvCB photosynthesis model, but also allows for a more realistic representation of such “memory”. Another advantage of the dynamic model is that it only requires values from the previous time step, not within the same time step calculations. Thus, the proposed equations (Eqn's 1–(6) are computationally inexpensive, requiring no additional numerical iteration for each time step. Even though the dynamic model is not fully mechanistic – e.g. it uses F_v/F_m as an empirical coupling factor – the relationships between chlorophyll fluorescence and irradiance response parameters do interact through mechanistic processes to account for photoinhibition response to multiple environmental variables (e.g. temperature and radiation).

Physiological modeling and land surface models (LSM) routinely use empirical relationships such as those proposed here: the Ball-Berry model (Ball et al., 1987); soil moisture or plant water status functions affecting photosynthetic parameters (e.g. Best et al., 2011; Medlyn et al., 2016; Medvigy et al., 2010; Vico and Porporato, 2008); the empirical application of two leaf models to multi-layer forests (e.g. Roy et al., 2012); the empirical support of the relationship of Φ_{PSII} to electron transport (e.g. Genty et al., 1989); models of photosynthetic and stomatal acclimation to elevated CO_2 (e.g. Ainsworth and Rogers, 2007); dynamics of stomata (Kirschbaum et al., 1997, 1988); the empirical relationship of V_{cmax} to J_{max} in LSM literature (e.g. Best et al., 2011; Walker et al., 2014); the non-mechanistic nature of FvCB parameters prior to the introduction of mesophyll limitations (Flexas and Medrano, 2002); empirical responses of stomata or mesophyll conductance to light (e.g. McAusland et al., 2016; Yin and Struik, 2009); the empirically based acceptance of a single value of mesophyll conductance, despite the poor representation of mesophyll conductance of sub-leaf level phenomena (Théroux-Rancourt et al., 2017), among others. Likewise, the advancements from our approach might only provide limited insights to answer fundamental physiological questions regarding biological mechanisms behind plant responses to environmental stress. However, the partly empirical nature of our model does not reduce the value of its prediction ability, nor its functional use until a more mechanistic improvement is made. For example, this approach would fit better the demands from climate models intending to represent the effects of temperature changes and drought on carbon fluxes than the steady state models currently in use.

5.5. Implementing and using the dynamic model

The dynamic modeling approach is based on the FvCB model, and thus, the standard calibration procedures apply for V_{cmax}, J_{max}, θ_{PSII} and $\Phi_{PSII,max}$. Usually, these last two components are not modeled as sensitive to temperature, but our data suggest that they should be considered as temperature sensitive parameters.

To account for stress in a dynamic fashion, a set of parameters for the relationship between irradiance response parameters and F_v/F_m is needed. Additionally, long term measurements of Φ_{PSII} might be needed if exploratory results show that time constants for almond photoinhibition mechanisms do not represent other species under investigation. The calibration of the dynamic model is possible using any PAM fluorometer system and leaf temperature measurement, as the model can be run off the variables it measures, without the need for further calibration of the FvCB model if one already exists for a species.

We expect that this model can be particularly useful for modeling plants that undergo sustained or severe stresses: boreal evergreens (Porcar-Castell et al., 2014), drought evergreens such as sclerophylls in Mediterranean ecosystems (Raab et al., 2015; Valladares and Pearcy, 1997, 2002), and plants with long cycles of water stress, or heat stress events. In addition, we expect that land surface and crop models would benefit of this approach by better representing gas exchange, biomass accumulation and surface temperature.

5.6. Concluding Remarks

A novel approach to dynamically model photosynthesis and photoinhibition is presented. Through a combination of field observation

and modeling techniques, we conclude that plant stress, damage, and recovery should be explicitly represented when modeling photosynthesis. From empirical relationships, our results showed clear signs of acclimation as a response to environmental stress, and such responses can have a long-term effect on photosynthesis. Stress responses and damage were well characterized by a relationship between irradiance response parameters and the fluorescence variable F_v/F_m. We expect that the combination of equipment able to monitor chlorophyll fluorescence continuously and a dynamic model of photosynthesis damage and recovery from stress will allow a more realistic representation of plant responses to environmental stress. This approach can be especially relevant when photosynthesis models are integrated within land surface schemes to dynamically model plant-atmosphere interactions in a changing climate. The proposed model is a starting point or framework, which we hope will initiate a conversation about shifting away from phenomenological models towards more mechanistic and dynamic modeling approaches capable of representing photosynthetic damage and physiological responses to stress.

Declaration of Competing Interest

The authors declare that they have no known competing financial interests or personal relationships that could have appeared to influence the work reported in this paper.

Acknowledgements

N.B. was supported by the Fulbright Program of Fellowships for Doctoral Studies, the Ernest E. Hill Research Award, and the National Science Foundation award EF1137306/MIT sub-award 5710003122 to the University of California Davis. M.E.G was supported by the USDA NIFA, Hatch project #1001480. Thanks to Guillaume Théroux-Rancourt and Thorsten Knipfer for comments on the manuscript.

Supplementary materials

Supplementary material associated with this article can be found, in the online version, at doi:10.1016/j.agrformet.2020.107911.

References

Aalto, J., et al., 2015. onset of photosynthesis in spring speeds up monoterpene synthesis and leads to emission bursts. Plant Cell Environ. 38 (11), 2299–2312.
Ainsworth, E.A., Rogers, A., 2007. The response of photosynthesis and stomatal conductance to rising [CO2]: mechanisms and environmental interactions. Plant Cell Environ. 30 (3), 258–270.
Baker, N.R., 2008. Chlorophyll fluorescence: a probe of photosynthesis in vivo. Annu. Rev. Plant Biol. 59, 89–113.
Ball, J.T., Woodrow, I.E., Berry, J.A., 1987. A model predicting stomatal conductance and its contribution to the control of photosynthesis under different environmental conditions. Progress in Photosynthesis Research. Springer, pp. 221–224.
Barber, J., 2009. Photosynthetic energy conversion: natural and artificial. Chem Soc Rev 38 (1), 185–196.
Berry, J.A., Downton, W.J.S., 1982. Environmental regulation of photosynthesis. Photosynthesis 2, 263–343.
Best, M.J., et al., 2011. . the joint uk land environment simulator (JULES), model description – Part 1: energy and water fluxes. Geoscientific Model Development 4 (3), 677–699.
Björkmann, O., Demmig, B., 1987. Photon yield of O2 evolution and chlorophyll fluorescence characteristics at 77K among vascular plants of diverse origins. Planta 170 (4), 489–504.
Correia, B., et al., 2014. Water stress and recovery in the performance of two eucalyptus globulus clones: physiological and biochemical profiles. Physiol Plantarum 150 (4), 580–592.
Demmig, B., Winter, K., Krüger, A., Czygan, F.-C., 1987. Photoinhibition and zeaxanthin formation in intact leaves. Plant Physiol. 84 (2), 218.
Demmig-Adams, B., Adams, W.W., 1996. The role of xanthophyll cycle carotenoids in the protection of photosynthesis. Trends Plant Sci. 1 (1), 21–26.
Egea, G., GonzÁLez-Real, M.M., Baille, A., Nortes, P.A., Diaz-Espejo, A., 2011. Disentangling the contributions of ontogeny and water stress to photosynthetic limitations in almond trees. Plant Cell Environ. 34 (6), 962–979.
Evans, J., 1987. The dependence of quantum yield on wavelength and growth irradiance. Functional Plant Biology 14 (1), 69–79.
Farquhar, G.D., Caemmerer, S., Berry, J.A., 1980. A biochemical model of photosynthetic CO2 assimilation in leaves of C3 species. Planta 149 (1), 78–90.
Flexas, J., Medrano, H., 2002. Drought-inhibition of photosynthesis in C3 plants: stomatal and Non-stomatal limitations revisited. Ann Bot-London 89 (2), 183–189.
Genty, B., Briantais, J.-.M., Baker, N.R., 1989. The relationship between the quantum yield of photosynthetic electron transport and quenching of chlorophyll fluorescence. Biochimica et Biophysica Acta (BBA)-General Subjects 990 (1), 87–92.
Goh, C.-.H., Ko, S.-.M., Koh, S., Kim, Y.-.J., Bae, H.-.J., 2012. Photosynthesis and environments: photoinhibition and repair mechanisms in plants. Journal of Plant Biology 55 (2), 93–101.
Horton, P., Wentworth, M., Ruban, A., 2005. Control of the light harvesting function of chloroplast membranes: the LHCII-aggregation model for non-photochemical quenching. FEBS Lett. 579 (20), 4201–4206.
Ivanov, A., Krol, M., Zeinalov, Y., Huner, N., Sane, P., 2008. The lack of LHCII proteins modulates excitation energy partitioning and PSII charge recombination in Chlorina F2 mutant of barley. Physiology and Molecular Biology of Plants 14 (3), 205–215.
Jahns, P., Holzwarth, A.R., 2012. The role of the xanthophyll cycle and of lutein in photoprotection of photosystem II. Biochimica et Biophysica Acta (BBA)-Bioenergetics 1817 (1), 182–193.
June, T., Evans, J.R., Farquhar, G.D., 2004. A simple new equation for the reversible temperature dependence of photosynthetic electron transport: a study on soybean leaf. Functional Plant Biology 31 (3), 275–283.
Kirschbaum, M., Küppers, M., Schneider, H., Giersch, C., Noe, S., 1997. Modelling photosynthesis in fluctuating light with inclusion of stomatal conductance, biochemical activation and pools of key photosynthetic intermediates. Planta 204 (1), 16–26.
Kirschbaum, M.U.F., Gross, L.J., Pearcy, R.W., 1988. Observed and modelled stomatal responses to dynamic light environments in the shade plant alocasia macrorrhiza. Plant Cell Environ. 11 (2), 111–121.
Krause, G., Weis, E., 1991. Chlorophyll fluorescence and photosynthesis: the basics. Annu Rev Plant Biol 42 (1), 313–349.
Kromdijk, J., et al., 2016. Improving photosynthesis and crop productivity by accelerating recovery from photoprotection. Science 354 (6314), 857–861.
Lin, Y.S., Medlyn, B.E., Ellsworth, D.S., 2012. Temperature responses of leaf net photosynthesis: the role of component processes. Tree Physiol. 32 (2), 219–231.
Long, S.P., Humphries, S., Falkowski, P.G., 1994. Photoinhibition of photosynthesis in nature. Annu Rev Plant Phys 45, 633–662.
Luo, H.-B., et al., 2011. Photosynthetic responses to heat treatments at different temperatures and following recovery in grapevine (Vitis amurensis L.) leaves. PLoS ONE 6 (8), e23033.
McAusland, L., et al., 2016. Effects of kinetics of light-induced stomatal responses on photosynthesis and water-use efficiency. New Phytologist 211 (4), 1209–1220.
Meacham, K.G., Sirault, X., Quick, W.P., von Caemmerer, S., Furbank, R.T., 2016. Diurnal solar energy conversion and photoprotection in rice canopies. Plant physiology: pp 01585, 2016.
Medlyn, B.E., De Kauwe, M.G., Duursma, R.A., 2016. New developments in the effort to model ecosystems under water stress. New Phytologist 212 (1), 5–7.
Medvigy, D., Wofsy, S.C., Munger, J.W., Moorcroft, P.R., 2010. Responses of terrestrial ecosystems and carbon budgets to current and future environmental variability. In: Proceedings of the National Academy of Sciences.
Müller, P., Li, X.-P., Niyogi, K.K., 2001. Non-photochemical quenching. a response to excess light energy. Plant Physiol. 125 (4), 1558–1566.
Nilkens, M., et al., 2010. Identification of a slowly inducible zeaxanthin-dependent component of non-photochemical quenching of chlorophyll fluorescence generated under steady-state conditions in Arabidopsis. Biochimica et Biophysica Acta (BBA)-Bioenergetics 1797 (4), 466–475.
Niyogi, K.K., 1999. Photoprotection revisited: genetic and molecular approaches. Annu Rev Plant Biol 50 (1), 333–359.
Ogren, E., Evans, J.R., 1992. Photoinhibition of Photosynthesis <I>in situ</I>in Six species of <I>Eucalyptus</I> Functional Plant Biology 19 (3), 223–232.
Öquist, G., Chow, W., Anderson, J.M., 1992. Photoinhibition of photosynthesis represents a mechanism for the long-term regulation of photosystem II. Planta 186 (3), 450–460.
Öquist, G., Huner, N.P., 2003. Photosynthesis of overwintering evergreen plants. Annu Rev Plant Biol 54 (1), 329–355.
Porcar-Castell, A., et al., 2014. linking chlorophyll a fluorescence to photosynthesis for remote sensing applications: mechanisms and challenges. Journal of Experimental Botany: eru 191.
R, Development_Core_Team, 2010. R: a language and environment for statistical computing. R Foundation for Statistical Computing, Vienna.
Raab, N., Meza, F.J., Franck, N., Bambach, N., 2015. Empirical stomatal conductance models reveal that the isohydric behavior of an Acacia Caven Mediterranean Savannah scales from leaf to ecosystem. Agric For Meteorol 213, 203–216.
Rivas, R., et al., 2017. Photosynthetic limitation and mechanisms of photoprotection under drought and recovery of calotropis procera, an evergreen C3 from arid regions. Plant Physiology and Biochemistry 118, 589–599.
Roháček, K., 2010. Method for resolution and quantification of components of the non-photochemical quenching (q N). Photosyn. Res. 105 (2), 101–113.
Roy, J., Ehleringer, J.R., Field, C.B., 2012. Scaling Physiological processes: Leaf to Globe. Academic Press.
Ruban, A.V., 2016. Nonphotochemical chlorophyll fluorescence quenching: mechanism and effectiveness in protecting plants from photodamage. Plant Physiol. 170 (4), 1903–1916.
Sharkey, T.D., Bernacchi, C.J., Farquhar, G.D., Singsaas, E.L., 2007. Fitting photosynthetic carbon dioxide response curves for C3 leaves. Plant Cell Environ. 30 (9), 1035–1040.
Théroux-Rancourt, G., et al., 2017. The bias of a two-dimensional view: comparing two-dimensional and three-dimensional mesophyll surface area estimates using

noninvasive imaging. New Phytologist 215 (4), 1609–1622.
Valladares, F., Pearcy, R., 1997. Interactions between water stress, sun-shade acclimation, heat tolerance and photoinhibition in the sclerophyll heteromeles arbutifolia. Plant Cell Environ. 20 (1), 25–36.
Valladares, F., Pearcy, R.W., 2002. Drought can be more critical in the shade than in the sun: a field study of carbon gain and photo-inhibition in a californian shrub during a dry el niño year. Plant Cell Environ. 25 (6), 749–759.
van der Tol, C., Verhoef, W., Rosema, A., 2009. A model for chlorophyll fluorescence and photosynthesis at leaf scale. Agric For Meteorol 149 (1), 96–105.
Vico, G., Porporato, A., 2008. Modelling c 3 and c 4 photosynthesis under water-stressed conditions. Plant Soil 313 (1–2), 187–203.
Virlouvet, L., et al., 2018. Dehydration stress memory: gene networks linked to physiological responses during repeated stresses of zea mays. Front Plant Sci 9.
Von Caemmerer, S., 2000. Biochemical Models of Leaf Photosynthesis. CSIRO Publishing, pp. 165.
Walker, A.P., et al., 2014. The relationship of leaf photosynthetic traits–Vcmax and jmax–to leaf nitrogen, leaf phosphorus, and specific leaf area: a meta-analysis and modeling study. Ecol Evol 4 (16), 3218–3235.
Webster, R.J. et al., 2016. High C3 photosynthetic capacity and high intrinsic water use efficiency underlies the high productivity of the bioenergy grass Arundo donax. 6: 20694.
Werner, C., Ryel, R.J., Correia, O., Beyschlag, W., 2001. Effects of photoinhibition on whole-plant carbon gain assessed with a photosynthesis model. Plant Cell Environ. 24 (1), 27–40.
Ye, Z.P., Suggett, D.J., Robakowski, P., Kang, H.J., 2013. A mechanistic model for the photosynthesis–light response based on the photosynthetic electron transport of photosystem II in C3 and C4 species. New Phytologist 199 (1), 110–120.
Yin, X., Struik, P.C., 2009. Theoretical reconsiderations when estimating the mesophyll conductance to CO2 diffusion in leaves of C3 plants by analysis of combined gas exchange and chlorophyll fluorescence measurements. Plant Cell Environ. 32 (11), 1513–1524.
Zhou, S., Medlyn, B., Sabate, S., Sperlich, D., Prentice, I.C., 2014. Short-term water stress impacts on stomatal, mesophyll and biochemical limitations to photosynthesis differ consistently among tree species from contrasting climates. Tree Physiol 34 (10), 1035–1046.